NANO LETTERS

pubs.acs.org/NanoLett Letter

Dispersion Mapping in 3-Dimensional Core–Shell Photonic Crystal Lattices Capable of Negative Refraction in the Mid-Infrared

Victoria F. Chernow,[⊥] Ryan C. Ng,*[,⊥] Siying Peng, Harry A. Atwater, and Julia R. Greer

Cite This: *Nano Lett.* 2021, 21, 9102–9107 Read Online

ACCESS | Metrics & More | Article Recommendations | Supporting Information

ABSTRACT: Engineering of the dispersion properties of a photonic crystal (PhC) opens a new paradigm for the design and function of PhC devices. Exploiting the dispersion properties of PhCs allows control over wave propagation within a PhC. We describe the design, fabrication, and experimental observation of photonic bands for 3D PhCs capable of negative refraction in the mid-infrared. Band structure and equifrequency contours were calculated to inform the design of 3D polymer–germanium core–shell PhCs, which were fabricated using two-photon lithography direct laser writing and sputtering. We successfully characterized a polymer–Ge core–shell lattice and mapped its band structure, which we then used to calculate the PhC refraction behavior. An analysis of wave propagation revealed that this 3D core–shell PhC refracts light negatively and possesses an effective negative index of refraction in the experimentally observed region. These results suggest that architected nanolattices have the potential to serve as new optical components and devices across infrared frequencies.

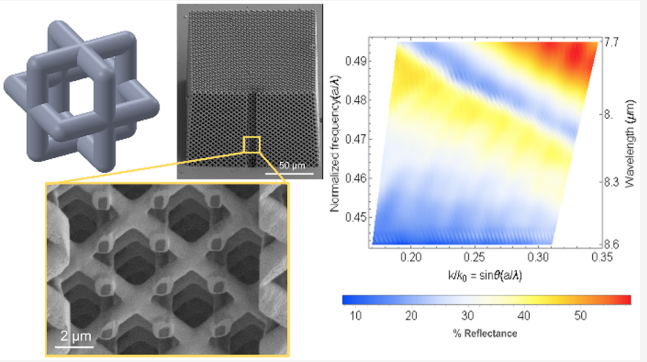

KEYWORDS: *photonic crystals, negative refraction, dispersion engineering*

The phenomenon of refraction describes the transmission behavior of a beam of radiation when it is incident on an interface between two materials. The direction of propagation of the transmitted beam will be modified relative to the indices of refraction of the two materials. Negative refraction (NR) is the phenomenon in which light bends in the opposite direction with respect to the surface normal at an interface, relative to what is observed in conventional materials. While it is not found naturally, this phenomenon is physically allowable. Veselago first proposed NR in 1968 and theorized that, if a material were to have simultaneously negative effective permittivity and permeability (a so-called "left-handed" material), the energy flow in the material, dictated by the Poynting vector, would be antiparallel to the wave vector.[1] This implies that in such a material the group velocity, $v_g = d\omega/dk$, is negative and that a refracted wave propagating away from the interface of this material would travel on the same side of the surface normal as the incident wave. A negative angle of refraction gives rise to a negative index of refraction.[2] Previous literature has shown that artificially prepared metamaterials and photonic crystals can exhibit NR.[3−13] Such negative index materials (NIMs) can act as superlenses, amplifying evanescent waves and potentially overcoming the diffraction limit inherent in conventional lenses.[14,15]

There are two means of achieving negative index materials. One requires a material to simultaneously possess a negative dielectric permittivity ε, and a negative magnetic permeability μ, where the vectors $\vec{E}$, $\vec{H}$, and $\vec{k}$ form a left-handed system, making a left-handed material. In the late 1990s, Pendry proposed that electromagnetic resonances in artificially engineered "metamaterials" made of periodic metal loops and wires could be tuned to values not accessible in natural materials.[14,16,17] The second means of obtaining a negative index is a photonic crystal (PhC) composed of purely dielectric, right-handed materials.[18] Both metamaterials and PhCs are artificial periodic structures that can control photons, yet PhCs operate at a wavelength on the order of their lattice constant. While NR in metamaterials is governed by effective medium theory, NR in PhCs arises from the dispersion characteristics of wave propagation in the periodic medium. In PhCs, theory and experiments have largely focused on achieving NR in 2D periodic structures, sufficient for the fabrication of superlenses capable of subwavelength imaging in a 2D plane.[6,12] Complete subwavelength imaging of 3D objects, however, requires a 3D PhC capable of negatively refracting light traveling in all three spatial planes. It was not until 2002 that Luo, Johnson, and Joannopoulos proposed a 3D lattice capable of NR for all incident angles from air, known

Received: July 22, 2021
Revised: October 13, 2021
Published: October 21, 2021

https://doi.org/10.1021/acs.nanolett.1c02851
Nano Lett. 2021, 21, 9102–9107

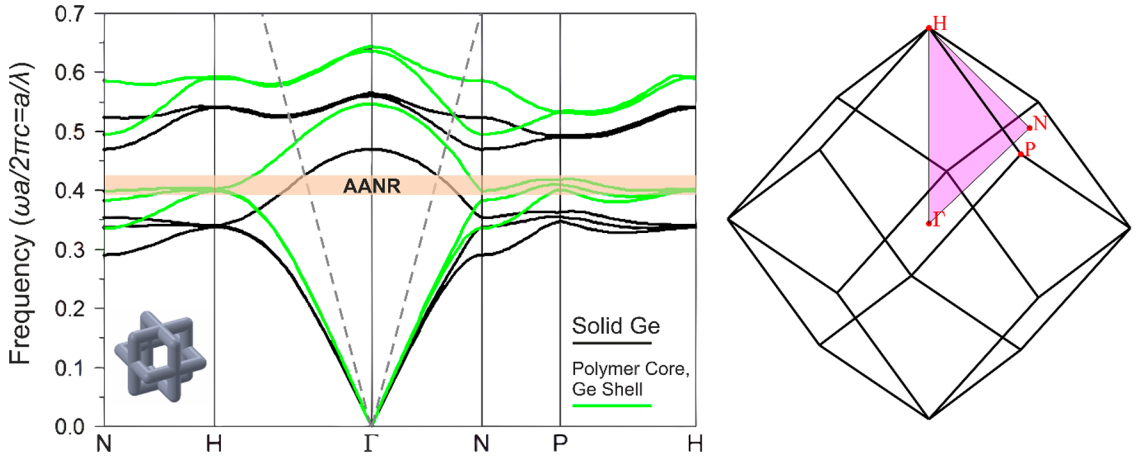

Figure 1. Band structure (black) of a 3D bcc PhC (f = 0.23) composed of fully dielectric beams with n = 4 (Ge at λ = 8 μm) and band structure (green) of a 3D bcc PhC (f = 0.23) composed of a 500 nm polymer core (n = 1.49) and 250 nm Ge shell (n = 4). The dashed gray lines are the light lines along ΓH and ΓN. The light orange band indicates the AANR region for solid Ge. A schematic of the unit cell is provided in the inset, and the first Brillouin zone is provided to the right of the band structure.

as all-angle negative refraction (AANR), though without an experimental demonstration.[19] A fully 3D structure is required to reach the AANR regime.

The structure proposed by Luo et al. consists of a body-centered cubic (bcc) lattice of air cubes embedded in a dielectric with ε = 18 (e.g., germanium, Ge, in the near-infrared).[19] For a conventional bcc unit cell with periodicity a, the sides of the air cube are parallel to the unit cell with edge length 0.75a. Their proposed PhC yields a band structure that possesses a negative photonic-mass region (concave-downward shape) in the third band between the ΓH and ΓN directions, where AANR is observed and the effective refractive index of the PhC is $n_{\text{eff}} \approx -1$ (refer to Figure 1 in ref 19). The frequency range for AANR in this lattice spans from $0.375(2\pi c/a)$ to $0.407(2\pi c/a)$, where the equifrequency contours (EFCs) of the third band are all-convex (circular) and larger than that of air (refer to Figure 2 in ref 19). The lower boundary of this AANR region falls at the frequency where the band has an inflection point, and the upper boundary is at the frequency where the band intersects the light line along the ΓH direction. This phenomenon occurs, in part, because of the large dielectric contrast between air and the high-index material comprising the PhC, with lower index materials reducing the observable frequency range for AANR while also shifting the AANR bounds to higher frequencies.[19]

Though this 3D PhC capable of AANR by Luo et al. was proposed theoretically, the only previous experimental demonstration of AANR in 3D to date was shown by Lu et al. at microwave frequencies, with milli-/centimeter sized features.[11,20] The lack of experiments demonstrating 3D NR in the optical and infrared ranges is largely due to difficulties in fabricating fully 3D lattices comprised of high-index materials (e.g., Ge) with features on the nano- and micrometer length scales. The advent of two-photon lithography (TPL) direct laser writing (DLW) has enabled the fabrication of arbitrarily complex 3D structures with sub-micrometer features generally in low-index polymeric scaffolds. This process combined with the deposition of high-index materials in techniques such as chemical vapor deposition (CVD) or sputtering provides a prospective route for the fabrication of 3D core−shell lattices capable of NR. Here, we design, fabricate, and measure a 3D architecture that exhibits negative refraction in the mid-IR regime, several orders of magnitude smaller than those in previous experimental demonstrations.

Figure 1 presents the photonic band structure diagrams for both a solid Ge 3D bcc PhC lattice (black) and a core−shell polymer−Ge (i.e., polymer scaffold with Ge coating) 3D bcc PhC lattice (green), along with the first Brillouin zone (right). The dashed gray lines are the light lines along high-symmetry directions in the first Brillouin zone of a bcc crystal. The light orange band highlights the AANR region for solid Ge. We used a plane-wave-expansion (PWE) method with the commercial software package RSOFT BandSOLVE to calculate the photonic band structure of the 3D PhCs in the mid-infrared using a bcc lattice based on the design proposed by Luo et al.[19] The inset in Figure 1 shows a representative lattice unit cell with cylindrical beams, rather than rectangular beams as used in Luo et al.,[19] to better reflect the topology of structures fabricated using TPL DLW, though the obtained band structures are qualitatively similar. The modeled PhCs in Figure 1 possess period a = 4 μm, an easily fabricated unit cell size using TPL DLW, and beam diameter b = 0.25a (volume fraction f = 0.23). For the solid beam 3D PhC, lattice beams are a single uniform material with dielectric constant ε = 16.038 (Ge in the mid-infrared around λ = 8.0 μm).[21] Our proposed PhC fabrication pathway involves first constructing a lattice out of a low-index polymer and then isotropically coating the structure with a high-index material; we carried out additional PWE band structure calculations to identify physically realizable lattice beam parameters for a core−shell PhC with appreciable AANR in the wavelength range between 7.7 and 8.62 μm. To maintain consistency with the previous monolithic Ge PhC band structure calculations, core−shell lattices retain the same periodicity of a = 4 μm and a total beam diameter of b = 0.25a = 1 μm (f = 0.23). The relative ratio of the low-index (n = 1.49) acrylate polymer core material[22] and high-index (n = 4.0047) Ge shell material[21] is varied by progressively increasing the core diameter and simultaneously shrinking the thickness of the shell to maintain the same total beam diameter. We observe a monotonic increase in the average frequency for AANR and a monotonic decrease in the AANR frequency range with decreasing compound refractive index of lattice beams. As the ratio of the core material to shell material increases, the combined

https://doi.org/10.1021/acs.nanolett.1c02851
Nano Lett. 2021, 21, 9102−9107

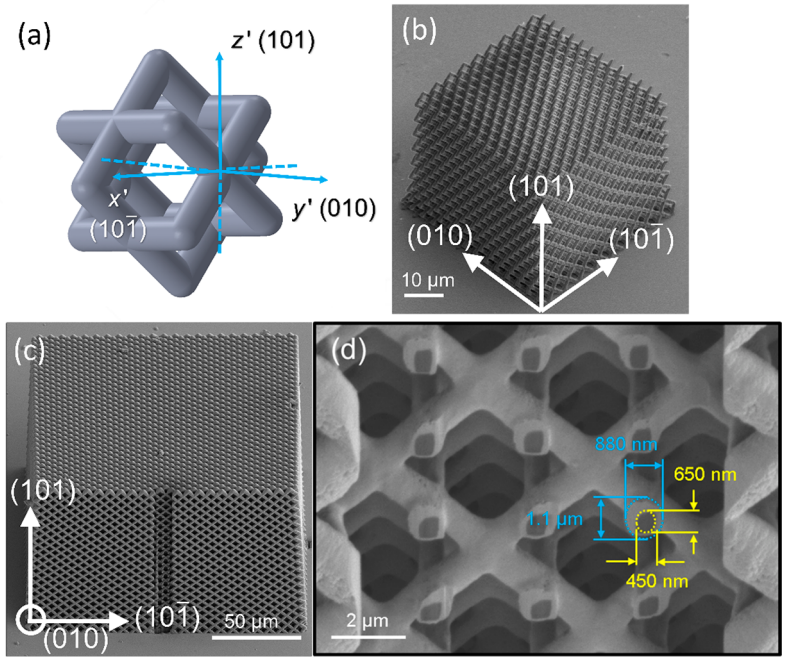

Figure 2. Proposed and fabricated 3D bcc PhC. (a) Proposed rotated bcc PhC unit cell with (101) surface orientation. (b) TPL DLW fabricated polymer PhC lattice with (101) surface orientation. (c) SEM image of the full core−shell lattice at a 52° tilt with FIB-milled cross-section. (d) Enlarged section of the PhC (010) face with approximate beam dimensions following a FIB cut into the lattice edge. Lateral and axial beam diameters are indicated for the inner (yellow) and outer (blue) beams.

index of the whole PhC eventually decreases below a threshold index, beyond which NR is no longer possible.[23] The band structure of the core−shell lattices is similar to those of the solid Ge PhCs, with additional bands at higher frequencies. A thorough analysis of the effect of effective index of refraction, beam ellipticity, and shell to core position offset on AANR can be found in Figures S1−S3 in the Supporting Information. These simulations revealed that, to observe AANR between 7.7 and 8.62 μm using polymer−Ge core−shell lattices, the core diameter should be no greater than ∼600 nm. This beam diameter is below the resolution limit of TPL DLW capability (cylindrical beams are limited to ∼900 nm diameter).

In our simulations aimed at identifying an AANR frequency region, we focused on the properties of the third band (as defined by band order from lowest to highest frequency), which possesses a concave-down shape indicative of a negative "photonic mass"[12,19] along the ΓN (101) direction. The AANR region is found between the point where the band intersects the light line and the point where the band curvature changes. In this frequency region, EFCs will be all-convex and larger than that of air, and the effective refractive index is $n_{\text{eff}} \approx -1$.[24] Above the light line, where band shape is still concave-down, the group velocity continues to be negative, but EFCs are no longer larger than that of air. Here, the effective refractive index will still be negative but is between $-1 < n_{\text{eff}} < 0$, and NR is now angle-dependent. Available optical characterization tools such as FTIR and angle-resolved spectroscopy only couple external radiation to leaky modes above the light line. Consequently, while we cannot directly access the PhC AANR region, we instead couple into band 3 above the light line, where the effective index is still negative between 0 and −1, although angle-dependent.

The proposed 3D bcc PhC lattice is fabricated in TPL DLW (see Figure 2 and the Supporting Information for full fabrication details). The fabricated lattices are constructed such that the original unit cell design (inset of Figure 1) is rotated by 45° around the y axis, so that the crystal surface is along the (101) direction (Figure 2a). To justify this design, we are reminded that the phenomenon of effective negative index in this bcc PhC lattice is present in a frequency range where band 3 specifically resides. The (101) direction (which corresponds to the PhC orientation and surface symmetry depicted in Figure 2b,c) refers to moving along the Γ−N high-symmetry direction and belongs to the C_{2v} symmetry group.[24] For this high-symmetry direction, the two potential polarizations of incident light interacting with the PhC are not degenerate, and the (10$\bar{1}$) polarization specifically can couple strongly to the PhC mode.[19] Conversely, for the other polarization along (010), coupling will be nonexistent at normal incidence and extremely low at nonzero incident angles.[19] Through group symmetry arguments, the NR phenomenon will be strongly dependent on PhC orientation and incident light polarization. Negative index behavior in our bcc PhC will be most obvious for a lattice with (101) surface termination and incident light of (10$\bar{1}$) polarization. We therefore fabricated our bcc PhC with the (101) orientation (Figure 2b) and remember these coupling restrictions in our experimental designs. Following TPL DLW fabrication, lattices possess circular beams with dimensions of ∼850−900 nm. From simulations, the polymer beam diameter must be <600 nm. Lattices were dry-etched with O_2 plasma to reduce the beam diameter. Figure 2c gives a representative SEM image of the (10$\bar{1}$) lattice face at a 45° tilt after 45 min of etching (Figure S4 in the Supporting Information). The etch rate is anisotropic with the transverse beam dimension etching more quickly and producing smaller features relative to the axial beam dimension. O_2 plasma etching yielded elliptical beams with short and long axes of 454 ± 27 and 647 ± 49 nm, respectively. The final fabrication step for low-index core−high-index shell bcc PhC lattices is the deposition of Ge onto

https://doi.org/10.1021/acs.nanolett.1c02851
Nano Lett. 2021, 21, 9102−9107

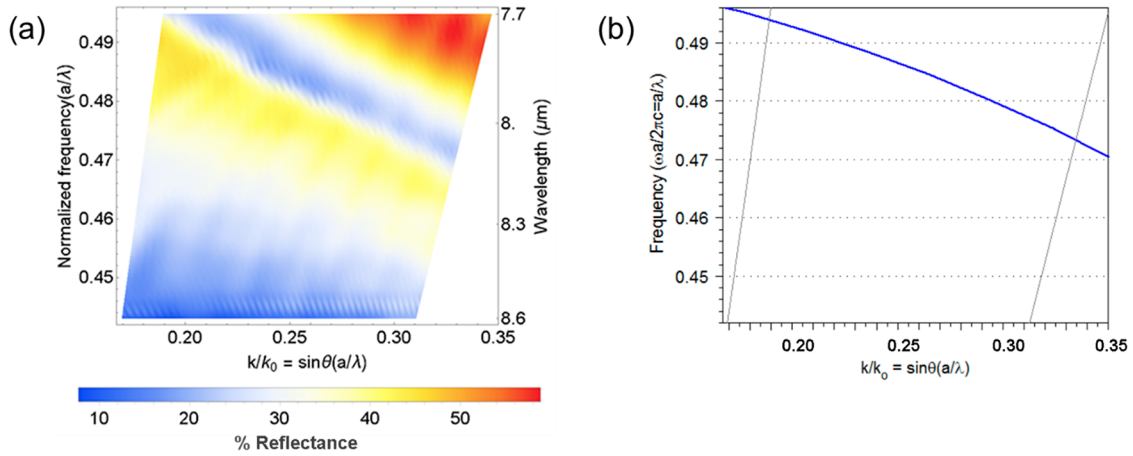

Figure 3. Experimentally measured and calculated band structures. (a) Angle-resolved reflectance measurement showing band 3 for the fabricated 3D core−shell bcc PhC. (b) Simulated band structure for the as-fabricated 3D core−shell bcc PhC with the same frequency and angle range as in (a).

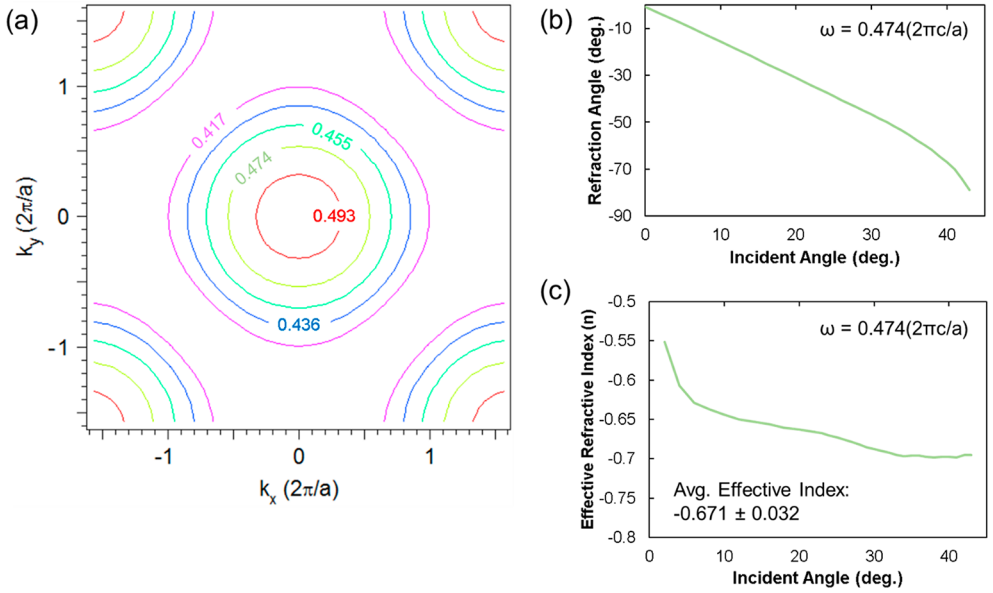

Figure 4. EFCs and resulting plots of NR and negative effective index. (a) Slice of the equifrequency surfaces on plane $k_z = 0$ for band 3 simulated in Figure 3b. The highest frequency circle is at the center (red). Subsequently lower frequencies have larger diameter contours, which indicates negative group velocity. (b) Refraction angle versus incident angle for $\omega = 0.474(2\pi c/a)$. (c) Effective refractive index as a function of incident angle for $\omega = 0.474(2\pi c/a)$.

the etched polymer scaffold. Roughly ∼250 nm thick Ge shells are deposited on the polymer lattice beams via a sputtering process optimized to maximize conformality, though chemical deposition techniques could improve this process. Focused ion beam (FIB) milling was used to assess the conformality and thickness of Ge deposited onto polymer lattices. To be as minimally destructive toward the sample as possible, only the edges of the core−shell PhC were FIB-milled for the measured sample, revealing beam cross sections for imaging and measurement with scanning electron microscopy (SEM) (Figure 2c). Additional edge cuts into the lattice during optimization showed that the dimensions do not vary significantly, with average dimensions being preserved. Figure 2d shows a cleaning cross-section FIB cut into the center of the (010) face of the core−shell PhC. We measure an average lattice period of 3.8 μm, likely from structure shrinkage during TPL DLW. In Figure 2d we cut approximately 1 μm into the PhC edge and observe (1) while Ge fully coats the polymer beams, it does not deposit isotropically, and an ∼200 nm offset in Ge shell position relative to polymer core position is evident, (2) beam cross sections are approximately elliptical with the long and short axes of the full beam measuring 1.1 μm and 880 nm, respectively, and (3) anisotropic etching of the polymer core is apparent at this cleaning cross-section depth and is approximated as elliptical with a short axis of 450 nm and a long axis of 650 nm. An average of the polymer core dimensions in comparison to the full core−shell beam dimensions provides the determination of an average Ge shell thickness of 255 nm, sufficient for observation of NR.

A negative effective index of refraction in these structures is demonstrated by experimentally mapping the photonic bands. As discussed previously, the band shape determines the shape of our EFCs and direction of the group velocity vector inside the PhC, providing the propagation direction of a refracted

https://doi.org/10.1021/acs.nanolett.1c02851
Nano Lett. 2021, 21, 9102−9107

beam. From Snell's law, an effective index of refraction for this 3D periodic architecture is then calculated at a given frequency. To truly observe and distinguish photonic states (i.e., photonic bands of our 3D core−shell PhCs), we require angle-resolved spectroscopic measurements and must selectively excite states at a precise momentum and wavelength. This is done in a quantum cascade laser (QCL) setup operating between 7.7 and 8.62 μm (see Figure S5 and Methods in the Supporting Information for measurement details).

For the angle-resolved reflectance measurements the incident laser light is polarized in the $[10\bar{1}]$ direction relative to the lattice, and interacts with the (101) PhC surface. The angular range covered in the experiments was limited from θ = 22.5° to 45° (θ is the angle between the incident beam and the normal to the crystal surface) due to limitations in the setup. The detector size prevented access below 22.5°. Above 45°, the reflectance signal was too low due to the smaller effective sample cross-section at large angles. Thus, the band structure of our bcc core−shell PhC was constructed from angle-resolved reflectance spectra captured between 22.5 and 45°. The inability to characterize at normal incidence or near the light line prevents direct access to the AANR region of the PhC. However, a concave-down curvature of the observable band implies a frequency region with a negative effective index between $-1 < n_{eff} < 0$.[19] Figure 3a shows the experimentally measured band structure for our core−shell PhC lattice. The emergence of a photonic mode is marked by a decrease in reflection intensity in the region between 7.7 and 8.1 μm that has concave-down character which replicates the appearance of the third band. The reflectance is relatively low between 8.3 and 8.62 μm due to absorption by the PhC's polymer core.[22] We compare the experimentally derived angle resolved band map (Figure 3a) to a PWE calculated band structure (Figure 3b). The simulated PhC accounted for structural features and lattice dimensions determined through FIB and SEM measurements. The unit cell size was set to 3.8 μm, and experimental imperfections were accounted for, yielding a representative core−shell PhC for simulation (see the Supporting Information for details on the simulation parameters). We calculate the band structure for this PhC approximation in the frequency range between $\omega = 0.441(2\pi c/a)$ and $\omega = 0.494(2\pi c/a)$ for angles between 22.5 and 45° along the ΓN direction, and the experimentally measured and simulated band structures show great agreement.

The EFCs for the band in Figure 3a are calculated in Figure 4a. The PhC contours are nearly circular and decreasing in radius as the frequency increases, implying NR. At the specific frequency $\omega = 0.474(2\pi c/a)$, we calculated how an incident wave is refracted within the PhC. From the EFC shape, we deduce the propagation angle using the relation $\vec{v}_g = d\omega/d\vec{k}$. Figure 4b shows the refraction versus incident angle for the EFC at $\omega = 0.474(2\pi c/a)$. At $\omega = 0.474(2\pi c/a)$ specifically, incident waves at angles >43° cannot couple to the PhC and will be totally reflected. The corresponding index for the refraction angle at this given frequency was then determined with Snell's law. Figure 4c plots the effective refractive index as a function of incident angle for $\omega = 0.474(2\pi c/a)$. Because the EFC at this frequency is not perfectly circular, the effective refractive index varies with the incident angle. However, the calculated effective index for our core−shell bcc PhC is negative, with an average value of $n_{eff} = -0.67$.

We have systematically analyzed the dispersion phenomena and NR properties of polymer−Ge core−shell PhCs in the mid-infrared using band theory and angle-resolved spectroscopy. Band structure calculations were performed to inform the design of the 3D PhC, which was subsequently fabricated using TPL DLW and sputtering. We successfully characterized a polymer−Ge core−shell lattice, mapped its band structure, and used this to calculate PhC refraction behavior. An analysis of wave propagation using EFCs revealed that this 3D core−shell PhC refracts light negatively and possesses an effective negative index of refraction in the experimentally mapped region. This work is the first experimental demonstration of negative refraction in 3D structures at such small length scales (i.e., mid-IR). All of the techniques and design rules implemented here could easily be used to further push AANR into the near-IR or visible regimes. This could be realized experimentally by incorporating pyrolysis or heat treatment to shrink the polymeric core lattices down to smaller length scales.[25−28] Alternatively, to circumvent complex fabrication procedures, advances in additive manufacturing[29−32] could further facilitate the fabrication and application of dispersion engineering in 3D PhCs.

■ ASSOCIATED CONTENT

Supporting Information

The Supporting Information is available free of charge at https://pubs.acs.org/doi/10.1021/acs.nanolett.1c02851.

Methods (sample fabrication, measurement), simulation parameters for comparison with the experimental band structure, and an analysis of AANR as a function of effective refractive index, beam ellipticity, and shell to core offset position (PDF)

■ AUTHOR INFORMATION

Corresponding Author

Ryan C. Ng − *Division of Engineering and Applied Sciences, California Institute of Technology, Pasadena, California 91125, United States; Division of Chemistry and Chemical Engineering, California Institute of Technology, Pasadena, California 91125, United States;* Present Address: Catalan Institute of Nanoscience and Nanotechnology, Bellaterra, Barcelona 08193, Spain; orcid.org/0000-0002-0527-9130; Email: rcng@caltech.edu

Authors

Victoria F. Chernow − *Division of Engineering and Applied Sciences, California Institute of Technology, Pasadena, California 91125, United States*

Siying Peng − *Division of Engineering and Applied Sciences, California Institute of Technology, Pasadena, California 91125, United States;* Present Address: Department of Materials Science and Engineering, Stanford University, Stanford, California 94305, USA.

Harry A. Atwater − *Division of Engineering and Applied Sciences, California Institute of Technology, Pasadena, California 91125, United States;* orcid.org/0000-0001-9435-0201

Julia R. Greer − *Division of Engineering and Applied Sciences, California Institute of Technology, Pasadena, California 91125, United States;* orcid.org/0000-0002-9675-1508

Complete contact information is available at: https://pubs.acs.org/10.1021/acs.nanolett.1c02851

Author Contributions

[⊥]V.F.C. and R.C.N. contributed equally.

Notes

The authors declare no competing financial interest.

■ ACKNOWLEDGMENTS

The authors gratefully acknowledge the financial support of the Dow-Resnick Grant, Defense Advanced Research Projects Agency, under the MCMA program managed by J. Goldwasser (Contract No. W91CRB-10-0305), and the U.S. Department of Energy (DOE) Office of Science (Grant No. DE-FG02-07ER46405). The authors also gratefully acknowledge the critical support and infrastructure provided by the Kavli Nanoscience Institute at Caltech.

■ REFERENCES

(1) Veselago, V. G. The Electrodynamics of Substances with Simultaneously Negative Values of ε and μ. *Sov. Phys. Uspekhi* **1968**, *10* (4), 509−514.
(2) Luo, C.; Johnson, S. G.; Soljacic, M.; Joannopoulos, J. D.; Pendry, J. B. Novel Optical Phenomena with Photonic Crystals. *Proc. SPIE* **2003**, *5166*, 207−219.
(3) Shalaev, V. M. Optical Negative-Index Metamaterials. *Nat. Photonics* **2007**, *1*, 41−48.
(4) Pendry, J. B. Negative Refraction. *Contemp. Phys.* **2004**, *45* (3), 191−202.
(5) Bang, S.; So, S.; Rho, J. Realization of Broadband Negative Refraction in Visible Range Using Vertically Stacked Hyperbolic Metamaterials. *Sci. Rep.* **2019**, *9* (14093), 1−7.
(6) Cubukcu, E.; Aydin, K.; Ozbay, E.; Foteinopoulou, S.; Soukoulis, C. M. Subwavelength Resolution in a Two-Dimensional Photonic-Crystal-Based Superlens. *Phys. Rev. Lett.* **2003**, *91* (20), 1−4.
(7) Gralak, B.; Enoch, S.; Tayeb, G. Anomalous Refractive Properties of Photonic Crystals. *J. Opt. Soc. Am. A* **2000**, *17* (6), 1012.
(8) Kosaka, H.; Kawashima, T.; Tomita, A.; Notomi, M.; Tamamura, T.; Sato, T.; Kawamaki, S. Superprism Phenomena in Photonic Crystals. *Phys. Rev. B* **1998**, *58* (16), R10096−R10099.
(9) Soukoulis, C. M.; Linden, S.; Wegener, M. Negative Refractive Index at Optical Wavelengths. *Science* **2007**, *315* (5808), 47−49.
(10) Shelby, R. A.; Smith, D. R.; Schultz, S. Experimental Verification of a Negative Index of Refraction. *Science* **2001**, *292* (5514), 77−79.
(11) Lu, Z.; Shi, S.; Schuetz, C. A.; Murakowski, J. A.; Prather, D. W. Three-Dimensional Photonic Crystal Flat Lens by Full 3D Negative Refraction. *Opt. Express* **2005**, *13* (15), 5592−5599.
(12) Luo, C.; Johnson, S. G.; Joannopoulos, J. D.; Pendry, J. B. All-Angle Negative Refraction without Negative Effective Index. *Phys. Rev. B: Condens. Matter Mater. Phys.* **2002**, *65* (20), 1−4.
(13) Zaremanesh, M.; Noori, M. All-Angle Polarization-Insensitive Negative Refraction in High-Dielectric Photonic Crystal. *Appl. Opt.* **2019**, *58* (21), 5631−5636.
(14) Pendry, J. B. Negative Refraction Makes a Perfect Lens. *Phys. Rev. Lett.* **2000**, *85* (18), 3966−3969.
(15) Liu, Z.; Fang, N.; Yen, T. J.; Zhang, X. Rapid Growth of Evanescent Wave by a Silver Superlens. *Appl. Phys. Lett.* **2003**, *83* (25), 5184−5186.
(16) Pendry, J. B.; Holden, A. J.; Stewart, W. J.; Youngs, I. Extremely Low Frequency Plasmons in Metallic Mesostructures. *Phys. Rev. Lett.* **1996**, *76* (25), 4773−4776.
(17) Pendry, J. B.; Holden, A. J.; Robbins, D. J.; Stewart, W. J. Magnetism from Conductors, and Enhanced Non-Linear Phenomena. *IEEE Trans. Microwave Theory Tech.* **1999**, *47* (11), 2075−2084.
(18) Notomi, M. Theory of Light Propagation in Strongly Modulated Photonic Crystals: Refractionlike Behavior in the Vicinity of the Photonic Band Gap. *Phys. Rev. B: Condens. Matter Mater. Phys.* **2000**, *62* (16), 10696−10705.
(19) Luo, C.; Johnson, S. G.; Joannopoulos, J. D. All-Angle Negative Refraction in a Three-Dimensionally Periodic Photonic Crystal. *Appl. Phys. Lett.* **2002**, *81* (13), 2352−2354.
(20) Lu, Z.; Murakowski, J. A.; Schuetz, C. A.; Shi, S.; Schneider, G. J.; Prather, D. W. Three-Dimensional Subwavelength Imaging by a Photonic-Crystal Flat Lens Using Negative Refraction at Microwave Frequencies. *Phys. Rev. Lett.* **2005**, *95* (15), 153901.
(21) Icenogle, H. W.; Platt, B. C.; Wolfe, W. L. Refractive Indexes and Temperature Coefficients of Germanium and Silicon. *Appl. Opt.* **1976**, *15* (10), 2348−2351.
(22) Chernow, V. F.; Alaeian, H.; Dionne, J. A.; Greer, J. R. Polymer Lattices as Mechanically Tunable 3-Dimensional Photonic Crystals Operating in the Infrared. *Appl. Phys. Lett.* **2015**, *107* (10), 101905.
(23) Chernow, V. F.; Ng, R. C.; Greer, J. R. Designing Core-Shell 3D Photonic Crystal Lattices for Negative Refraction. *Proceedings of SPIE - The International Society for Optical Engineering* **2017**, 101120G.
(24) Dresselhaus, M. S.; Dresselhaus, G.; Jorio, A. *Group Theory - Application to the Physics of Condensed Matter*; Springer Berlin Heidelberg: 2008.
(25) Gailevičius, D.; Padolskytė, V.; Mikoliūnaitė, L.; Šakirzanovas, S.; Juodkazis, S.; Malinauskas, M. Additive-Manufacturing of 3D Glass-Ceramics down to Nanoscale Resolution. *Nanoscale Horizons* **2019**, *4*, 647−651.
(26) Seniutinas, G.; Weber, A.; Padeste, C.; Sakellari, I.; Farsari, M.; David, C. Beyond 100 nm Resolution in 3D Laser Lithography — Post Processing Solutions. *Microelectron. Eng.* **2018**, *191*, 25−31.
(27) Sun, Q.; Juodkazis, S.; Murazawa, N.; Mizeikis, V.; Misawa, H. Freestanding and Movable Photonic Microstructures Fabricated by Photopolymerization with Femtosecond Laser Pulses. *J. Micromech. Microeng.* **2010**, *20* (3), 035004.
(28) Liu, Y.; Wang, H.; Ho, J.; Ng, R. C.; Ng, R. J. H.; Hall-Chen, V. H.; Koay, E. H. H.; Dong, Z.; Liu, H.; Qiu, C. W.; Greer, J. R.; Yang, J. K. W. Structural Color Three-Dimensional Printing by Shrinking Photonic Crystals. *Nat. Commun.* **2019**, *10*, 4340.
(29) Vyatskikh, A.; Delalande, S.; Kudo, A.; Zhang, X.; Portela, C. M.; Greer, J. R. Additive Manufacturing of 3D Nano-Architected Metals. *Nat. Commun.* **2018**, *9* (593), 1−8.
(30) Vyatskikh, A.; Ng, R. C.; Edwards, B.; Briggs, R. M.; Greer, J. R. Additive Manufacturing of High-Refractive-Index, Nanoarchitected Titanium Dioxide for 3D Dielectric Photonic Crystals. *Nano Lett.* **2020**, *20* (5), 3513−3520.
(31) Camposeo, A.; Persano, L.; Farsari, M.; Pisignano, D. Additive Manufacturing: Applications and Directions in Photonics and Optoelectronics. *Adv. Opt. Mater.* **2019**, *7* (1), 1800419.
(32) Bourell, D. L. Perspectives on Additive Manufacturing. *Annu. Rev. Mater. Res.* **2016**, *46* (3), 1−18.

https://doi.org/10.1021/acs.nanolett.1c02851
Nano Lett. 2021, 21, 9102−9107